Supplementary Information

The Effect of Electrolyte Alkali Cation on CO_2 Electroreduction in Atomically Precise $Ag_{25}(SR)_{18}$ Nanoclusters

Yuting Ye[a] [+], Xia Zhou[b] [+], Yuping Chen[a], Likai Wang*[b] and Qing Tang*[a]

[a] School of Chemistry and Chemical Engineering, Chongqing Key Laboratory of Chemical Theory and Mechanism, Chongqing University, Chongqing 401331, China

[b] School of Chemistry and Chemical Engineering, Shandong University of Technology, Zibo, Shandong, 255049, China

[+] These authors contributed equally to this work.

*To whom correspondence should be addressed. E-mail: lkwangchem@sdut.edu.cn; qingtang@cqu.edu.cn

Chemicals and materials.

Silver nitrate ($AgNO_3$, AR), tetraoctylammonium bromide (TOAB, 98%), 2,4-dimethylbenzenethiol ($HSPhMe_2$, 95%), tetraphenylphosphonium bromide (PPh_4Br, 98%), Sodium borohydride ($NaBH_4$, AR), Potassium chloride (KCl, AR), Sodium Chloride (NaCl, AR), Lithium chloride (LiCl, AR), Nafion solution (5 wt%), tetrahydrofuran (THF, AR), methanol, dichloromethane (CH_2Cl_2, AR) and ethanol were used without further purification.

Electrochemical measurements.

The catalytic activity of Ag_{25} NCs was obtained using an electrochemical workstation (CHI 760E) with a three-electrode system coupled to a CO_2 flow cell. The electrolyte solutions were 0.5 M NaCl, 0.5 M KCl and 0.5 M LiCl solutions, and the reference electrode was an Ag/AgCl electrode (immersed in saturated KCl solution), an anion-exchange membrane, and a platinum plate used as the ion mobility channel and counter electrode, respectively. The working electrode was prepared as follows: 1

mg carbon nanotube and 1 mg Ag_{25} NCs were dissolved in 0.5 mL of CH_2Cl_2 to achieve a uniform dispersion ink containing 10 μL of 5 wt% Nafion solution, 0.5 mL of the above solution was sprayed onto 1 cm^2 (GDL) with the loading mass of 2 mg/cm^2.

The cathodic electrolyte was continuously saturated with CO_2 for 30 min before electrochemical CO_2 reduction reaction (eCO_2RR). The cathode and anode reaction chambers are separated by a proton exchange membrane (Nafion-115) placed in a neutral medium. In the electrocatalytic reduction process, each electrolyte cell contained 30 mL of electrolyte, which was circulated by a peristaltic pump at 40 rpm from the flow chamber to the corresponding electrolyte cell. The gas products were analyzed quantitatively and qualitatively with the aid of a gas chromatograph (GC, Huaai 9560).

The potential in this work is converted to reversible hydrogen electrode (RHE) potential according to the equation:

$$E(RHE) = E(Ag/AgCl) + 0.197V + 0.0591 \times pH$$

Faraday efficiency of gas products was calculated based on the following formula (FE):

$$FE = \frac{Q_i}{Q_{total}} = \frac{N_i \times Z \times F}{Q_{total}}$$

where Q_i is the charge required to form the gaseous product, Q_{total} is the total charge during the reaction, N_i is the number of moles of the product detected by gas chromatography, Z is the number of electrons transferred during the formation of the product (2 for CO and H_2), and F is Faraday's constant (96485 C mol^{-1}).

Calculation of the turnover frequency (TOF) was as follow:

$$TOF(h^{-1}) = \frac{j_i/ZF}{m_i * \omega/M} \times 3600$$

where j_i is the partial current density of the corresponding gas product, Z is the number of transferred electrons formed by the product (2 for CO), F is the Faraday constant (96485 C mol^{-1}), m_i is the mass of the loading catalyst, ω is the relative mass fraction of Ag in the catalyst, and M is the relative atomic mass of Ag. Linear sweep voltammetry (LSV) was conducted in a 1 M KOH solution saturated with either N_2 or

CO_2, using a scan rate of 50 mV s^{-1}.

The CO_2-to-CO conversion overpotentials (η) were then calculated using the following equation:

$$\eta = E_{SHE} - E_{eq}$$

$$E_{SHE} = E_{RHE} + 0.0591\,V$$

Where η is the overpotential (in V), E_{eq} is the equilibrium potential for CO_2 reduction to CO, which is approximately –0.11 V (vs. the standard hydrogen electrode, SHE).

The Tafel slopes of selective Ag_{25} samples for CO_2RR were obtained from the linear region of the low-overpotential region, using the following equation.

$$\eta = a + b\,log\,|j_{CO}|$$

where η is the overpotential, b is the Tafel slope, j is the current density. Linear fitting was performed in the region where log $|j_{CO}|$ versus η exhibited linearity, avoiding the mass transport-limited region.

Free Energy Calculations. The kinetic barriers are obtained by applying a holonomic constraint on the reaction coordinate (ζ) during constrainted AIMD simulations.[1]

For H adsorption on the S site, the distance between S and H atoms is chosen as the collective variable (CV), which is defined by eq 1:

$$CV = \zeta(r) = |r_{OH} - r_{SH}| \quad (1)$$

where r_{OH} refer to the coordinates of the O atom of H_2O and the H atom of H_2O, and r_{SH} refer to the coordinates of the S atom of Ag_{25} and the H atom of H_2O (*COOH, *CO, *H adsorption; *H desorption is similar).

For -SCH_3 ligand removal from the metal site, the CV is defined by eq 2:

$$CV = \zeta(r) = |r_{Ag} - r_S| \quad (2)$$

where r_{Ag} refer to the coordinates of the Ag atom and r_S refer to the coordinates of the S atom of Ag_{25}.

For CO_2 adsorption on the metal site, the CV is defined by eq 3：

$$CV = \zeta(r) = |r_{Ag} - r_C| \quad (3)$$

where r_{Ag} and r_C refer to the coordinates of the metal atom and the C atom of CO_2 (*CO desorption is similar).

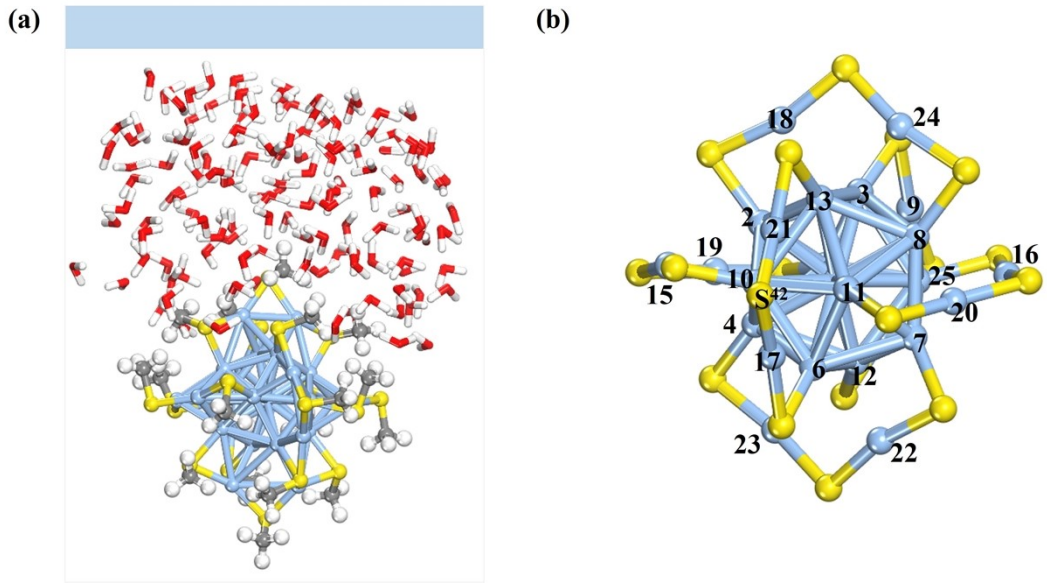

Figure S1. Theoretical modeling of Ag_{25}/water interface in the neutral system (a) and the metal core structure and corresponding atomic numbers of the Ag_{25} (b) cluster. Ag, C, S, O and H atoms are colored with blue, grey, yellow, red and white, respectively (similarly hereinafter).

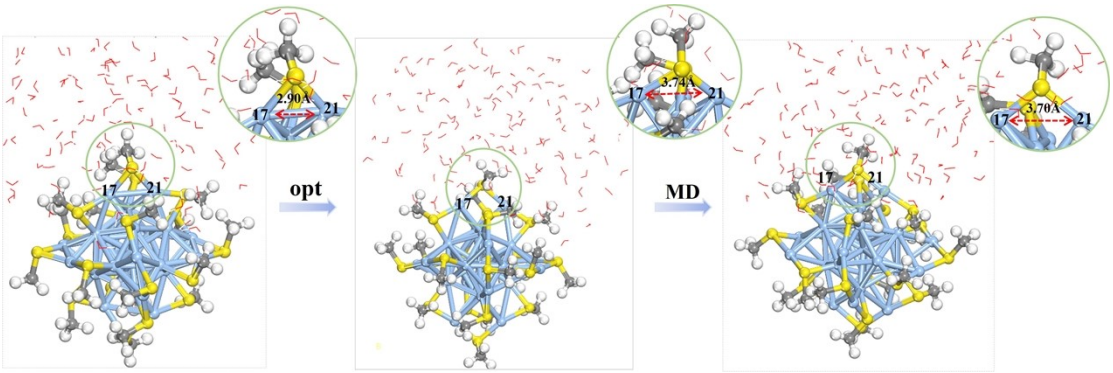

Figure S2. Optimization and Dynamic Equilibrium simulation of the Ag_{25}/water interface under Cation-Free Conditions.

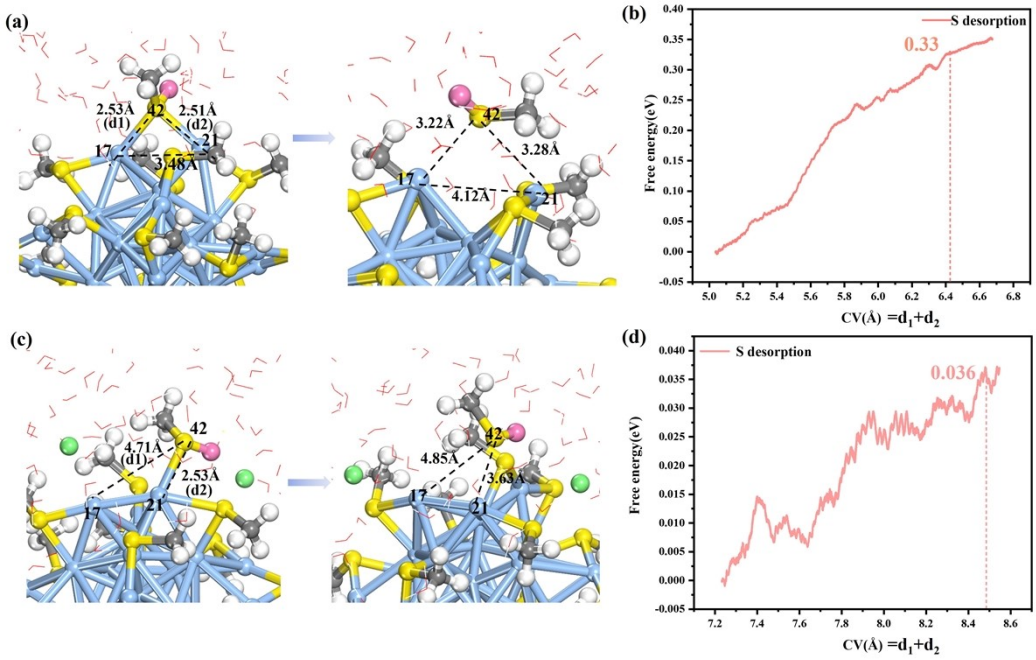

Figure S3. Snapshot of S desorption and the corresponding free energy during the SR removal of Ag_{25} nanocluster in the water (a, b) and Li^+ (c, d) environment, obtained via constrained AIMD simulations at 300 K under pH=7 conditions. Ag, C, S, O, Li, H and adsorbed H atoms are colored with blue, grey, yellow, red, green, white and pink, respectively (similarly hereinafter).

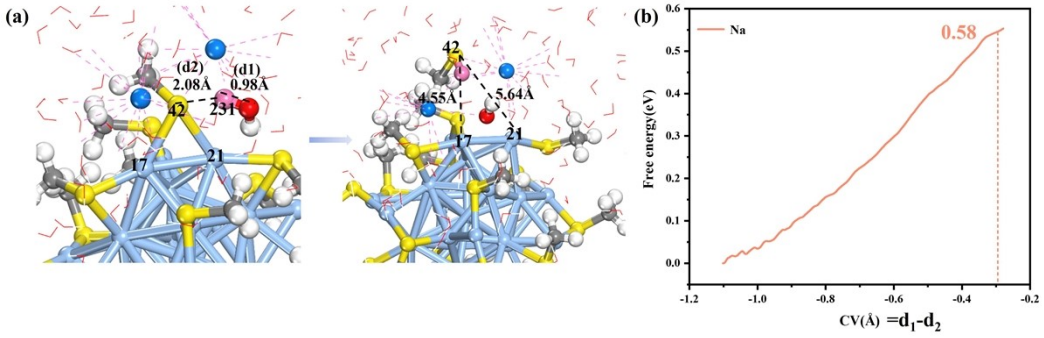

Figure S4. Schematic illustration (a) of the SR removal process for Ag_{25} nanoclusters in the presence of Na^+, obtained via constrained AIMD simulations under conditions of pH = 7 and 300 K, along with the corresponding free energy (b). Na^+ is colored with blue.

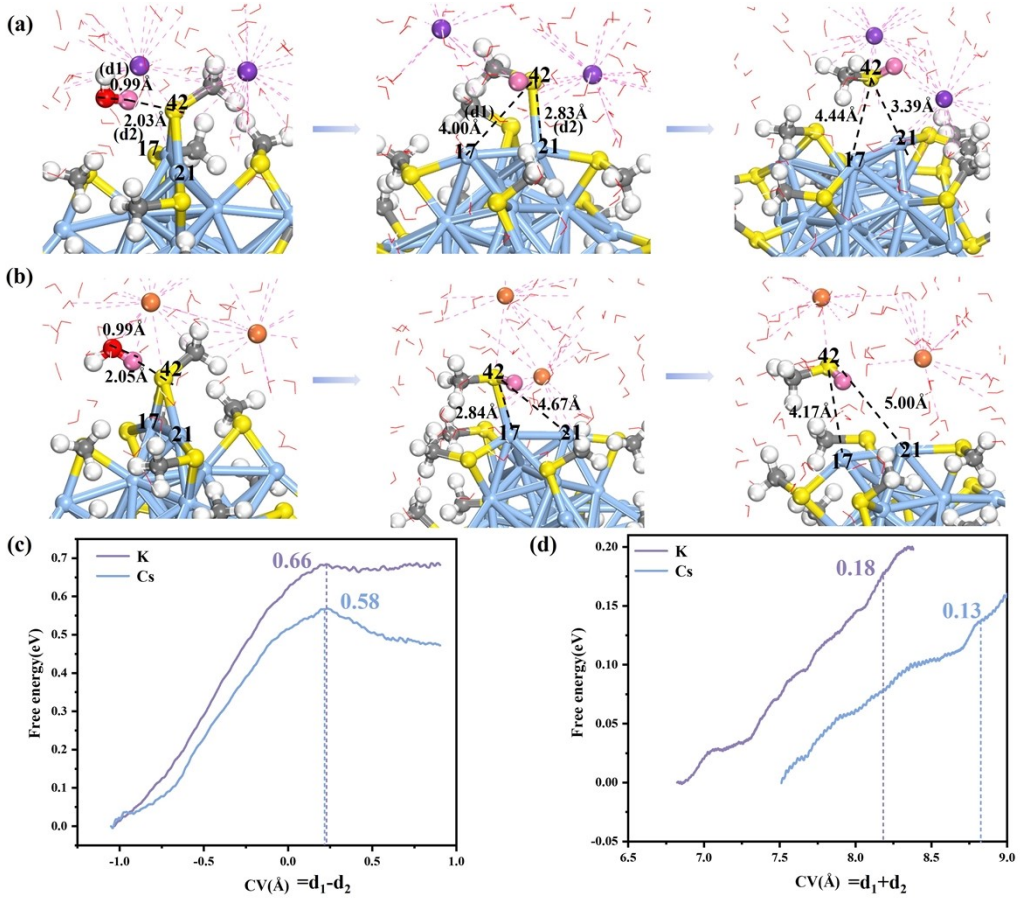

Figure S5. Schematic illustration of the SR removal process for Ag_{25} nanoclusters in the presence of K^+ (a) and Cs^+ (b); as well as the corresponding free energy of SR removal in K^+ (c) and Cs^+ (d). K^+ and Cs^+ are colored with purple and orange, respectively.

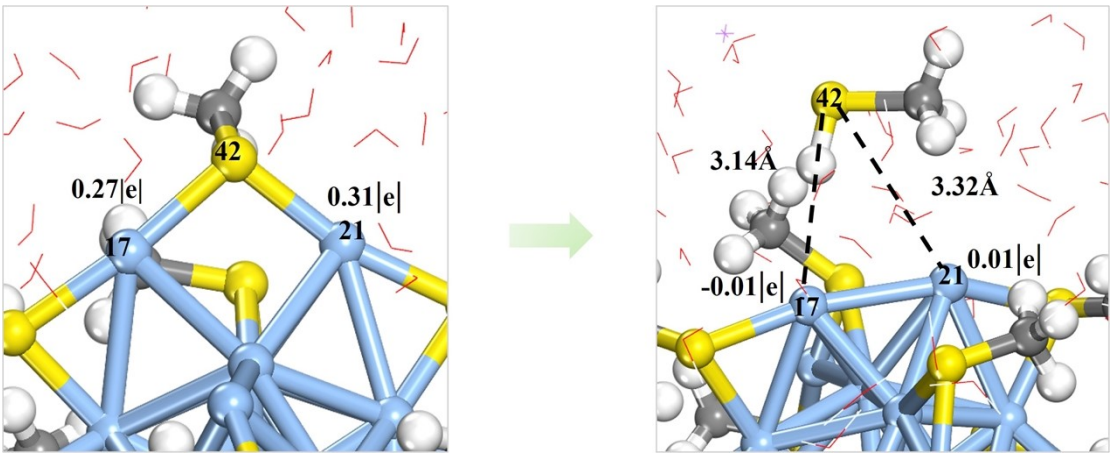

Figure S6. Bader charges of Ag_{17} and Ag_{21} atoms in intact $Ag_{25}(SCH_3)_{18}$ and dethiolated $Ag_{25}(SCH_3)_{17}$ as well as the corresponding local magnification images.

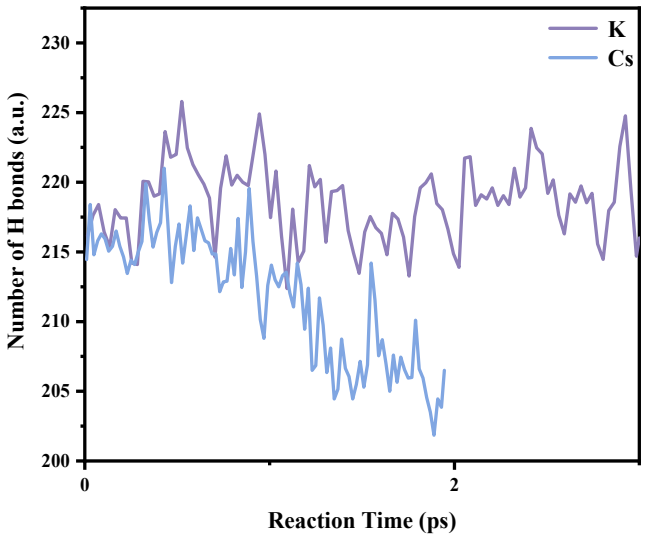

Figure S7. Schematic illustration of the number of hydrogen bonds formed during the formation of the *COOH intermediate in the presence of K^+ and Cs^+.

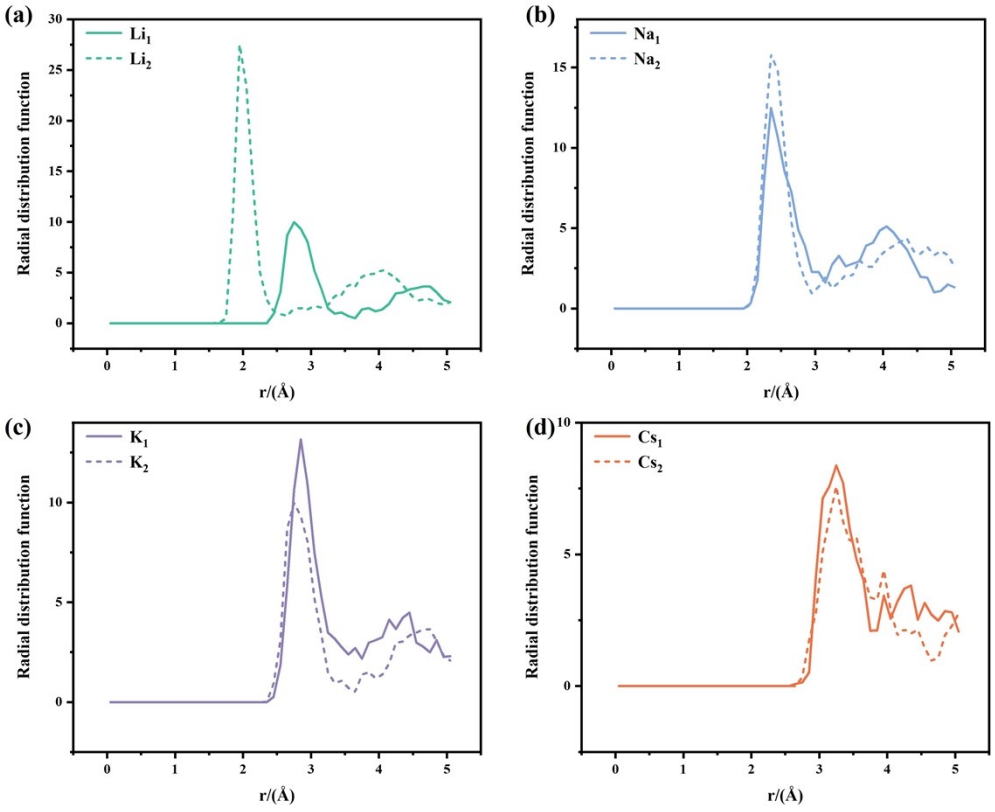

Figure S8. The radial distribution functions (RDF) of Li^+ (a), Na^+ (b), K^+ (c), and Cs^+ (d) with oxygen atoms from surrounding H_2O during the *COOH formation step (solid and dashed lines

represent M_1 and M_2 in the unified model, M=cations).

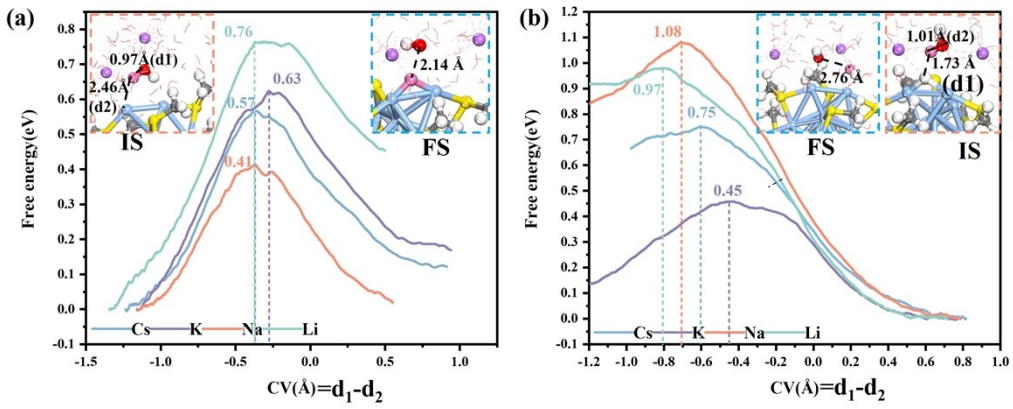

Figure S9. Comparison of the integral free energy curves of *H formation (a) and *H desorption to form H_2 (b) in the presence of Li^+, Na^+, K^+, and Cs^+ environment by constrained AIMD simulations. The local structures of initial state (IS), final state (FS) and the defined collective variable (CV, d_1-d_2) are shown inset.

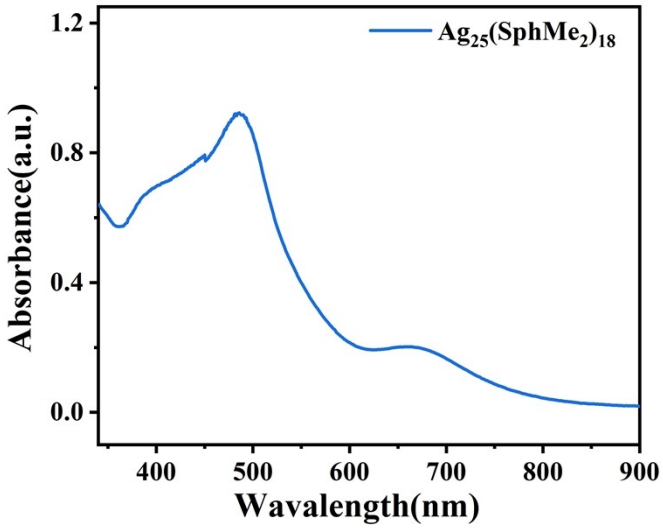

Figure S10. UV-vis spectra of $Ag_{25}(SPhMe_2)_{18}$.

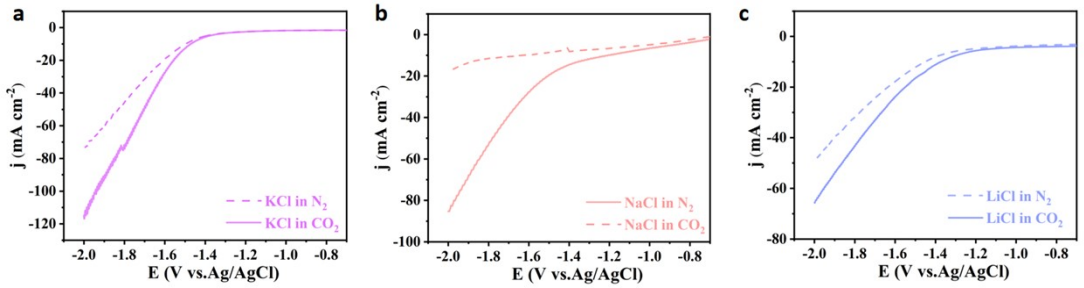

Figure S11. LSV measurements of Ag_{25} in N_2 and CO_2 conditions with 0.5 M KCl (a), 0.5 M NaCl (b) and 0.5 M LiCl (c).

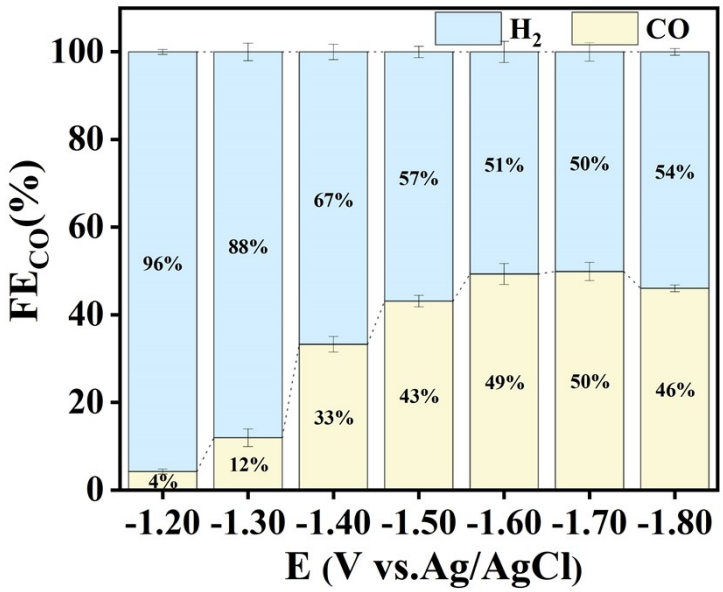

Figure S12. FE_{CO} of Ag_{25} in the flow cell under CO_2 atmosphere with 0.5 M CsCl conditions.

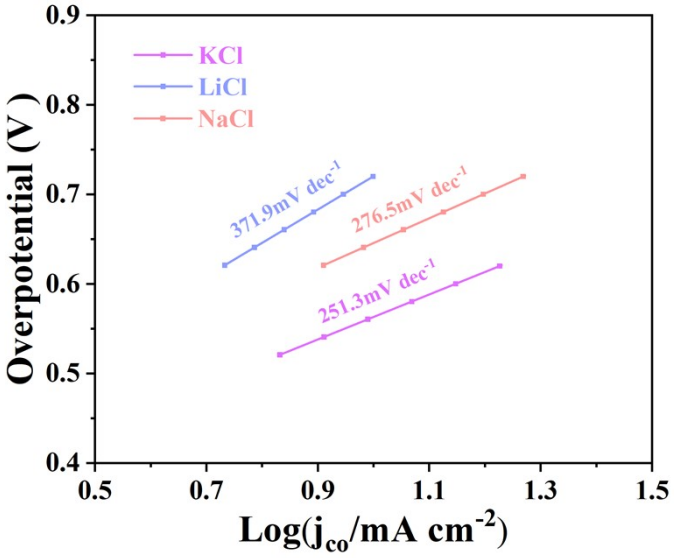

Figure S13. Tafel plots of Ag_{25} in 0.5 M KCl, NaCl and LiCl electrolytes.

Table S1. Bader charges of Ag atoms in intact $Ag_{25}(SCH_3)_{18}$ and dethiolated $Ag_{25}(SCH_3)_{17}$. The Bader charge of exposed under-coordinated Ag atoms are marked in orange.

Atom	Before site removal	After site removal
Ag^{1}	-0.05	-0.06
Ag^{2}	0.10	0.11
Ag^{3}	0.13	0.09
Ag^{4}	0.12	0.14
Ag^{5}	0.13	0.12
Ag^{6}	0.12	0.08
Ag^{7}	0.13	0.08
Ag^{8}	0.12	0.10
Ag^{9}	0.14	0.11
Ag^{10}	0.11	0.09
Ag^{11}	0.11	0.11
Ag^{12}	0.14	0.16

Ag^{13}	0.27	0.27
Ag^{14}	0.28	0.24
Ag^{15}	0.27	0.30
Ag^{16}	0.32	0.27
Ag^{17}	0.27	-0.01
Ag^{18}	0.30	0.29
Ag^{19}	0.29	0.28
Ag^{20}	0.15	0.09
Ag^{21}	0.31	0.01
Ag^{22}	0.30	0.27
Ag^{23}	0.28	0.27
Ag^{24}	0.28	0.28
Ag^{25}	0.27	0.26

References

(1) Cao, H.; Zhang, Z.; Chen, J.-W.; Wang, Y.-G. Potential-dependent free energy relationship in interpreting the electrochemical performance of CO_2 reduction on single atom catalysts. *ACS Catal.* **2022**, *12* (11), 6606-6617.